Joint Centre for Mesoscale Meteorology, Reading, UK

A classification of FASTEX cyclones using a height-attributable QG vertical motion diagnostic

A. C. L. Deveson
K. A. Browning
T. D. Hewson

Internal Report No. 120
NWP Scientific Paper No. 57

September 7, 2000

Met Office Joint Centre for Mesoscale Meteorology Department of Meteorology
University of Reading PO Box 243 Reading RG6 6BB United Kingdom
Tel: +44 (0)118 931 8425 Fax: +44 (0)118 931 8791
www.metoffice.com

Designed and produced by the Met Office © Crown copyright 2001 01/0240 The Met Office logo is a registered trademark.

A classification of FASTEX cyclones using a height-attributable QG vertical motion diagnostic.

A.C.L. Deveson, K.A. Browning and T.D. Hewson

September 7, 2000

Abstract

A systematic and objective method is developed for applying the simple cyclone classification scheme developed by Petterssen and Smebye (1971). This method uses a height-attributable solution of the quasi-geostrophic (QG) ω equation to identify and quantify the relative importance of upper- and lower-tropospheric forcing and also the time trend in the horizontal spacing of the forcing at these two levels. By applying this classification method to an unbiased sample of cyclogenesis events from the FASTEX field experiment, the Type A and Type B scheme of Petterssen and Smebye (1971) is reproduced and extended to include a Type C. Type C, consists of upper-level dominated cyclones that form at high latitudes and in their initial stages resemble comma-cloud type polar lows. Detailed examples of each of the three types are presented. Some cyclones can undergo more than one period of development and it is found that each development period can be classified as a different cyclogenesis category, A or B: these cyclones are classified as hybrid Type A/B. Evidence is given that the forecast accuracy of cyclones depends on their type, thereby suggesting the potential for this method to be used to assign confidence levels for forecasts of cyclogenesis produced by numerical weather prediction models. Type B cyclones appear more difficult to predict, because their development depends, initially, on the interaction between significant features in the upper and lower troposphere.

1 Introduction

The Fronts and Atlantic Storm-Track Experiment (FASTEX) took place in January and February 1997. In-situ observations were taken of 24 cyclogenesis events that occurred over the North Atlantic basin. As well as observing selected cyclones in detail, extra radiosonde ascents were taken around the perimeter of the North Atlantic and on ships straddling the main baroclinic zone to provide an enhanced description of the background flow. See Joly *et al.* (1997), (1999) for overviews of the FASTEX experiment.

One of the objectives of FASTEX was to verify cyclogenesis theories using the large database of cyclogenesis events in the North Atlantic basin. Joly *et al.* (1999) and Baehr *et al.* (1999) have categorised cyclones during FASTEX using new criteria, but no attempt has been made to verify existing classification schemes using the FASTEX database. The present paper uses data from FASTEX to examine the validity and usefulness of the well-known synoptic classification scheme of Petterssen and Smebye (1971).

Classification schemes have been developed to systematise and help understand the variability in the structure, strength, scale and life-time of extra-tropical cyclones. Recent synoptic classification schemes use satellite imagery and synoptic observations to categorise cyclogenesis. The scheme developed by McLennan and Neil (1988) is an example of one such scheme that has been developed specifically for use as an alternative forecasting tool to numerical weather prediction (NWP) models. The most recently developed synoptic classification schemes, such as those by Evans *et al.* (1994) and Young (1993) (also in Bader *et al.* (1995)), classify cyclones using two approaches. They classify cyclones according to their cloud configurations using work by Weldon (1979). They also classify cyclones in terms of the interactions between the upper-level trough and low-level cyclone. The latter approach is based on the concept introduced by Petterssen *et al.* (1955) that extra-tropical cyclogenesis involved vertical as well as lateral interactions. Based on the results from observational studies Petterssen *et al.* (1955) and Petterssen *et al.* (1962), Petterssen went on to develop the first synoptic classification scheme (Petterssen and Smebye (1971), hereafter referred to as PS71). This was a simple classification scheme with only two categories, A and B, in contrast to Young's (1993) scheme which has 7 types of extra-tropical cyclogenesis. Table 1 summarises the classification scheme developed by PS71 in terms of vorticity advection and thermal advection as well as the general synoptic situation. However, as with all synoptic classification schemes, the systematic application of even these rather simple ingredients is

Type A	Type B
Synoptic Situation: Cyclone forms on a front. No pre-existing upper-level trough. A trough may form as the cyclone intensifies. The distance between trough and cyclone remains constant until peak intensity is reached.	**Synoptic situation:** Cyclone forms when an upper-level trough moves over a region of warm advection. The axis of the system tends to the vertical as the cyclone intensifies. Distance between trough and cyclone decreases rapidly as cyclone intensifies.
Vorticity Advection: Initially very small at upper-levels. Although it increases as the cyclone develops, it remains relatively small.	**Vorticity Advection:** Initially very large at upper-levels. It decreases as peak intensity is approached.
Thermal Advection: Very large at low-levels and the main contributer to the cyclone's intensification.	**Thermal Advection:** Initially small at low-levels, it increases as the cyclone intensifies.

Table 1: A summary of the classification scheme developed by Petterssen and Smebye (1971).

difficult and subjective. There have also been very few cyclones reported in the literature that could be categorised as Type A since the publication of PS71.

The present study also uses the PS71 classification scheme as its starting point. An objective method to apply this scheme has been developed using a height-attributable solution of the quasi-geostrophic ω equation. Owing to the large number of extra observation assimilated during FASTEX, high-quality NWP analyses are available for a large sample of cyclones. Diagnostics derived from operational NWP model output are therefore used to provide the objective method of applying the classification scheme.

This paper is structured as follows. In Sec. 2, the height-attributable solution to the quasi-geostrophic ω equation is introduced. A new systematic method for applying the PS71 classification scheme using the height-attributable vertical motion diagnostic is described. Then idealised Type A and Type B cyclones are described in terms of the classification method. In Sec. 3 results are shown from applying this method to 16 cyclogenesis events that occurred during FASTEX. This leads to the identification of several Type A and Type B cyclones and of another category of cyclones referred to as Type C. Finally, in Sec. 4, an example from each category is examined in more detail. Throughout this paper cyclones are referred to by the designated "Low" number from the FASTEX experiment.

2 A Method for using height-attributable ω_{QG} to classify cyclones.

he classification scheme developed by PS71, as shown by Table 1, can be viewed in terms of the vorticity advection (VA) and thermal advection (TA). The quasi-geostrophic (QG) ω equation relates VA and TA to vertical motion (ω_{QG}). PS71 showed that in Type B cyclones where VA at upper levels dominated then the vertical motion maximum was at upper levels whereas in a case of cyclogenesis with similarities to Type A cyclogenesis the vertical motion maximum was at a much lower level. Therefore it can be assumed that in terms of the classification scheme by PS71 the vertical motion due to VA can be considered to be equivalent to the upper-level forced ω_{QG} diagnostic while the vertical motion due to TA can be considered to be equivalent to the lower-level forced ω_{QG} diagnostic. The assumption that thermal advection at upper levels and vorticity advection at lower levels is negligible has, historically, frequently been assumed when examining the vertical motion

structure of extra-tropical cyclones. However, to the author's knowledge, no quantitative assessment of this assumption has been made. Nevertheless, it will be assumed here that vorticity advection dominates the vertical motion forced from upper levels and that thermal advection dominates the vertical motion forced from lower levels since we are comparing new techniques to existing ones which also made this assumption. This means that using the ω_{QG} diagnostics an objective and systematic method for applying the classification scheme by PS71 can be developed.

2.1 Height-attributable ω_{QG}

The full QG ω equation can be written as follows:

$$N^2\nabla_h^2\omega + f_0^2\frac{\partial}{\partial z}\left(\frac{1}{\rho_s}\frac{\partial}{\partial z}(\rho_s\omega)\right) = 2\nabla_h.\mathbf{Q} \tag{1}$$

where ω is the quasi-geostrophic vertical velocity $\frac{dz}{dt}$ (hereafter referred to as ω_{QG}), z is the height-like pressure coordinate defined by Hoskins and Bretherton (1972) and N is the reference Brunt-Väisälä frequency which is dependent only on height. ρ_s is the reference density profile as defined in Equation 2.

$$\rho_s = \rho_0 \exp\left(-\frac{z}{H_\rho}\right) \tag{2}$$

$\mathbf{Q}$ is the Q vector as defined by Hoskins *et al.* (1978) while ∇_h is the horizontal gradient on a constant-z surface.

A method of solving equation 1 that enables vertical motion at any point in space to be attributed to the temperature and wind structure within user-specified layers, or "slabs" of the atmosphere has been developed by Clough and Davitt (1994) and Clough *et al.* (1996). This involved solving the ω equation by applying the electrostatic analogy as introduced by Thorpe and Bishop (1995). When solving the ω equation in this manner there is a reduced sensitivity to small-scale features and sources close to the boundaries, including the surface (see Clough *et al.* (1996) for details). As ω_{QG} is being used here to examine synoptic-scale features associated with cyclogenesis, this reduced sensitivity to small-scale features does not restrict its use. However, the solution of the the ω equation is domain dependent. This is because the quasi-geostrophic assumption requires static stability to be constant in the horizontal. In calculating the ω_{QG} diagnostics, a domain-averaged static stability is used at every level.

Figure 1 shows the distribution of ω_{QG} due to a "ball" source of forcing for vertical motion of radius 125km located at 500hPa as calculated by Clough *et al.* (1996). This shows that a source of ω_{QG} 125km in radius, of similar magnitude to a synoptic feature, can affect the vertical velocity field out to 1000km in the horizontal and over the whole depth of the atmosphere. Using traditional methods of estimating vertical motion from the QG ω equation, such as the convergence of Q vectors, this source of ω_{QG} would be included in the Q vectors calculated only at 500hPa, even though it influences the whole depth of the atmosphere. However, by solving the QG ω equation in the manner proposed by Clough and Davitt (1994) and Clough *et al.* (1996), ω_{QG} can be calculated at all points, with contributions from all sources of vertical motion. Height-attribution can be achieved by calculating ω_{QG} forced only from specified layers of the atmosphere.

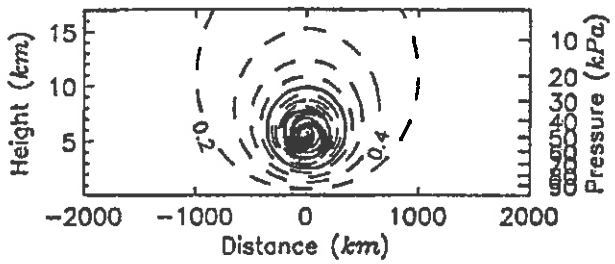

Figure 1: Vertical motion distribution attributable at 45°N to a 125km radius ball-source of $2\nabla_h.\mathbf{Q} = -8 \times 10^{-14} m^{-1} s-3$ at 500hPa. Contours are at intervals of $0.2 cms^{-1}$ (dashed) and $1 cms^{-1}$ (solid). After Clough *et al.* (1996).

An example of an extra-tropical cyclone, Low 33 from FASTEX, is now used to explain how this diagnostic can be applied to examine cyclogenesis. Figure 2(a) shows Low 33 at 12UTC 8 Feb.97, the time of maximum rate of deepening. The geopotential height at 1000hPa and 300hPa are shown in order to represent the structure of the low-level cyclone and upper-level trough, respectively. The potential vorticity (PV) contour at 400hPa corresponding to 1PV unit is also shown to indicate the location of the positive upper-level PV anomaly associated with the development. The location of a cross-section through the system has been added. Figure 2(b) shows this cross-section from south-west to north-east. Plotted on the cross-section are contours of PV greater than 1PVU, and also the ω_{QG} forced from the layer 1050 to 750hPa (defined as "lower levels") and the ω_{QG} forced from the layer 650 to 50hPa (defined as "upper levels").

It can be seen from Fig. 2(b) that the ω_{QG} distributions forced from both upper and lower levels, respectively extends beyond each of these layers, and indeed overlap each other at

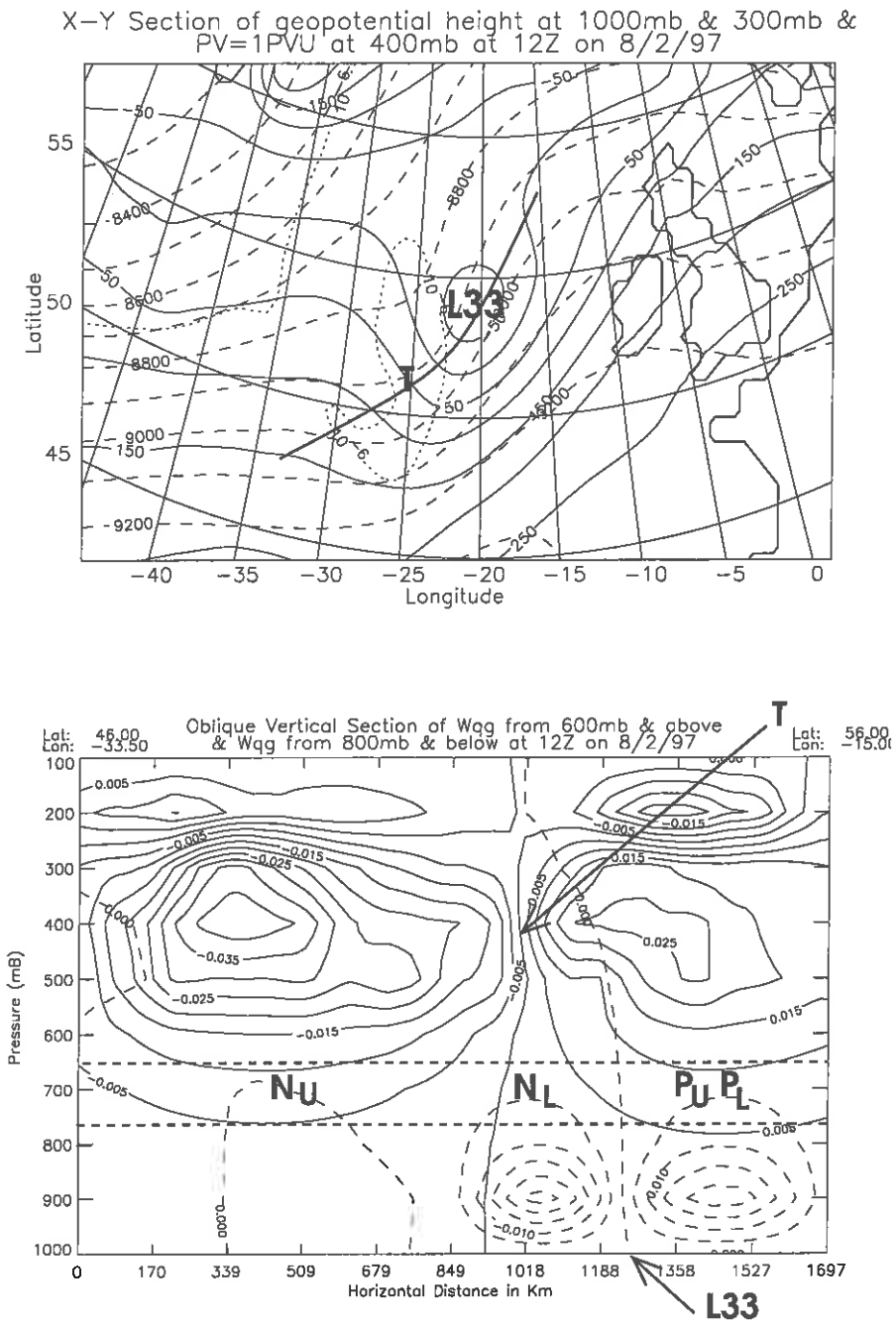

Figure 2: Diagnostics from Low 33 at 12UTC on 8 Feb. 97. (a) Geopotential height at 1000hPa (solid contours) and 300hPa (dashed contours) and PV greater than 1PVU at 400hPa (dotted contours). Thick solid line represents location of the cross-section. (b) Cross-section, along the direction of travel of Low 33, through upper-level trough and low centre, showing PV the ω_{QG} forced from between 600 and 100hPa (dashed contours at intervals of $0.005ms^{-1}$) and the ω_{QG} forced from between 1000 and 800hPa (solid contours at intervals of $0.005ms^{-1}$). L33 represents the location of the surface low pressure centre and T the location of through the upper-level trough axis on the cross-section. P_U, N_U and P_L, N_L represent the location of the ascent and descent maxima at 700hPa forced from upper levels and lower levels respectively. The bold dashed lines represent the lower and upper limits, respectively, of the sources of upper and lower-level forcing of ω_{QG}.

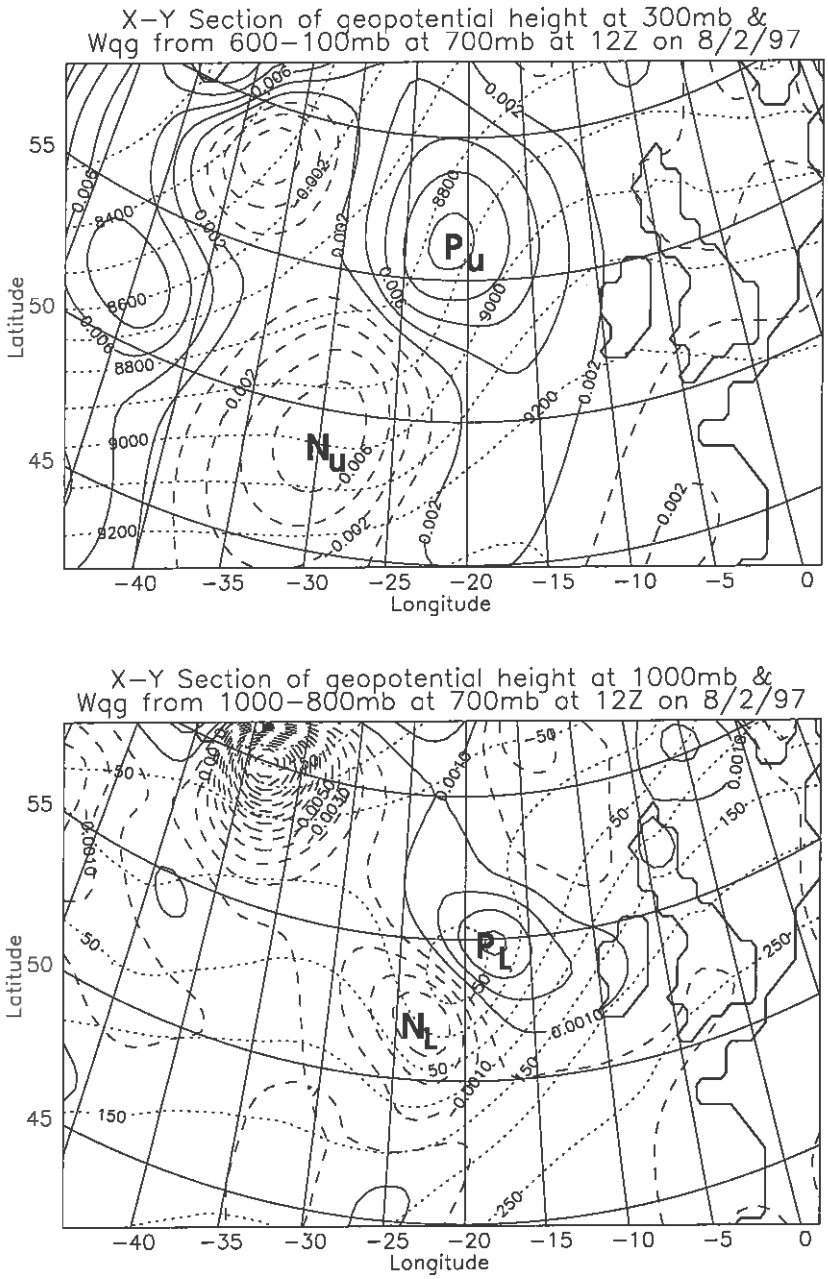

Figure 3: Further diagnostics of Low 33 at 12UTC on 8 Feb. 97. (a) ω_{QG} at 700hPa forced from levels between 600hPa and 100hPa inclusively with solid contours for ascent and dashed contours for descent at intervals of $0.002ms^{-1}$, overlaid with 300hPa geopotential height (dotted contours). (b)ω_{QG} at 700hPa forced from levels between 1000hPa and 800hPa inclusively with solid contours for ascent and dashed contours for descent at intervals of $0.002ms^{-1}$, overlaid with 1000hPa geopotential height (dotted contours). P_U, N_U and P_L, N_L represent the location of the ascent and descent maxima at 700hPa forced from upper levels and lower levels, respectively.

700hPa. Four points have been labelled on Fig. 2(b). They represent the maximum positive and negative upper-level forced ω_{QG} at 700hPa, labelled P_U and N_U respectively, and the maximum positive and negative lower-level forced ω_{QG} at 700hPa, labelled P_L and N_L respectively. Table 2 gives the values of ω_{QG} at these points. From this table it can be seen that at this time the ω_{QG} at 700hPa forced from upper levels was greater than the ω_{QG} at 700hPa forced from lower levels. Therefore it could be said that at this time in the cyclone development it was predominantly upper-level forced (accepting that there is some arbitrariness in the choice of 700hPa as the mid-tropospheric reference level).

Date	P_U	N_U	P_L	N_L
12z 8/2/97	1.05	-0.74	0.42	-0.40

Table 2: Values of the maximum and minimum vertical velocity in cms^{-1} forced from upper levels (P_U and N_U) and lower levels (P_L and N_L) at 700mb at 12UTC 8 Feb. 97 in association with Low 33.

Figure 3(a) displays the upper-level forced ω_{QG} at 700hPa superimposed on the 300hPa geopotential height field from Fig. 2(a). Similarly Fig. 3(b) displays the lower-level forced ω_{QG} at 700hPa superimposed on the 1000hPa geopotential height from Fig. 2(a). The ω_{QG} dipoles associated with the upper-level trough and the low-level cyclone can clearly be identified and the maxima in ascent and descent are labelled P_U, N_U, P_L and N_L as in Fig. 2(b). The ω_{QG} dipole in Fig. 3(a) is related to the vorticity advection associated with the trough axis. Analysis of this and other events shows that maxima in ω_{QG} at 700hPa corresponding to points P_U and N_U can always be identified if such an upper-level trough is present. Similarly the points P_L and N_L can always be identified in the low-level forced ω_{QG} field at 700hPa if there is a low-level cyclone present, because the ω_{QG} dipole in Fig. 3(b) is produced by the thermal advection around the cyclone. This means that, by locating the ω_{QG} dipoles forced from upper and lower levels at 700hPa, the upper-level trough and low-level cyclone can be tracked and the relative strengths of the associated forcing can be quantified. At present these points are tracked manually, with their magnitude and relative location noted every three hours. This reduces the objectivity of using this diagnostic. However, it would be possible to adapt an automatic tracking routine such as that developed by Hodges (1994) to track these features.

The ω_{QG} diagnostics are calculated throughout this paper from output from the UKMO limited area model (LAM) that was operational during 1997 (Panagi and Dicks, 1997) . The full LAM domain includes a large area of land. This means that the domain-averaged static-stability profile used in calculating ω_{QG} is not representative of an oceanic region, where the case studies we shall be examining occurred. Therefore, from now on in this paper, ω_{QG} will be shown using the DISP display system which uses a reduced domain and interpolates LAM output on to a polar stereographic grid with a resolution of 100hPa in the vertical and approximately 100km in the horizontal (Roberts, 1998) . This domain is centred on the North Atlantic and is more appropriate for examining cyclones crossing this region. Although DISP calculates the ω_{QG} diagnostics at a lower horizontal resolution than possible with the original LAM output, this was found not to alter significantly the synoptic-scale features of the ω_{QG} distribution.

2.2 New method for applying the classification scheme of Petterssen and Smebye

The criteria distinguishing Type A and Type B cyclogenesis as defined by PS71 in table 1 can be re-expressed as:

- Does an upper-level trough pre-exist the initiation of low-level cyclogenesis? **Yes - B; No - A**

An upper-level trough is defined to be associated with a low-level cyclone if there exists an upper-level forced ω_{QG} dipole at 700mb with the ascent maximum downstream of the descent maximum close within 2000km of the low-level cyclone.

- Does the separation between the upper-level trough and cyclone remain constant or decrease as the cyclone intensifies? **Constant - A; Decrease - B**

The way in which this is assessed is described below.

- Does vorticity advection (VA) at upper-levels or thermal advection (TA) at lower-levels dominate? **VA - B; TA - A**

This is assessed by means of a ratio of the height-attributable ω_{QG} diagnostics referred to as the **The U/L ratio.** This is the ratio of "forcing for vertical motion at 700hPa attributable

to **upper levels (and therefore mainly to the VA associated with the upper-level trough)" to "forcing for vertical motion at 700hPa attributable to lower levels (and therefore mainly to the TA associated with the low-level cyclone)". This ratio shows whether upper-level forced or lower-level forced ω_{QG} dominates the cyclogenesis event. The evolution of this ratio can be viewed to see how the cyclone evolves during cyclogenesis. An averaged value can also be calculated to summarise the forcing regime throughout the cyclogenesis event. The life-time of a cyclogenesis event was taken as starting when the 900hPa relative-vorticity maximum increased to over $8.0 \times 10^{-5} s^{-1}$ and ended when it reached its maximum intensity while within the LAM domain. The average U/L ratio was calculated as follows. First the magnitude of the upper-level forced ω_{QG} dipole was calculated by summing the magnitudes of the maximum ascent and maximum descent at 700hPa from the upper level (referred to as he upper-level dipole strength, $|D_U|$, hereafter). The lower-level dipole strength, $|D_L|$, was calculated in a similar fashion. The U/L ratio of the upper- and lower-level dipole strength ($\frac{|D_U|}{|D_L|}$) was then calculated at each time step. To give equal weighting to values of the ratio above and below 1.0, the natural log of the ratios was taken. The exponential of the average of the logged ratios was then used to represent the dominant forcing during a cyclogenesis event. Although the time-averaged U/L ratio does not show the variation in the forcing during cyclogenesis, we shall show that it clearly distinguishes between the different regimes that can occur.

Vertical tilt of forcing To represent the tilt between the upper-level trough and low-level cyclone, the distance between the ascent maxima at 700hPa forced from upper levels and lower levels is measured. This is given as positive if the upper-level forced ascent maximum was to the west or north of the cyclone and negative if to the south or east. It was found that the upper-level forced ascent maximum was always initially to the north or west of the cyclone but could overtake the cyclone. This is not the traditional "tilt" measured in baroclinic systems. Instead, it is the displacement between the maximum forcing for ascent from upper levels and lower levels, felt at 700hPa. This displacement or vertical tilt of forcing is being used here to quantify the distance between the upper-level trough and low-level cyclone as discussed by PS71. If a cyclone falls into the PS71 Type B category then it is expected that the separation distance should decrease as the cyclone intensifies. Therefore, for Type B cyclones, a negative correlation should be expected between the cyclone intensity (given by the 900hPa maximum relative vorticity) and the tilt value. No such correlation is expected in Type A cyclones. The least-squares correlation coefficient,

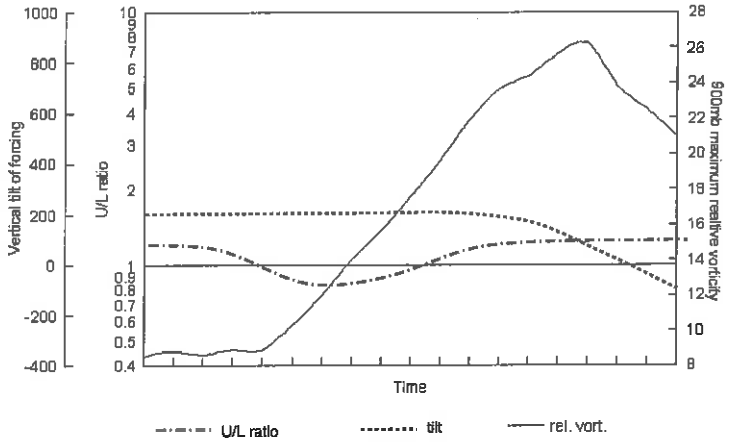

Figure 4: Graphs showing the time-history of the U/L ratio and vertical tilt of the forcing (in km), and also the 900hPa maximum relative vorticity (rel. vort. in $\times 10^{-5} s^{-1}$) for an idealised Type A cyclone.

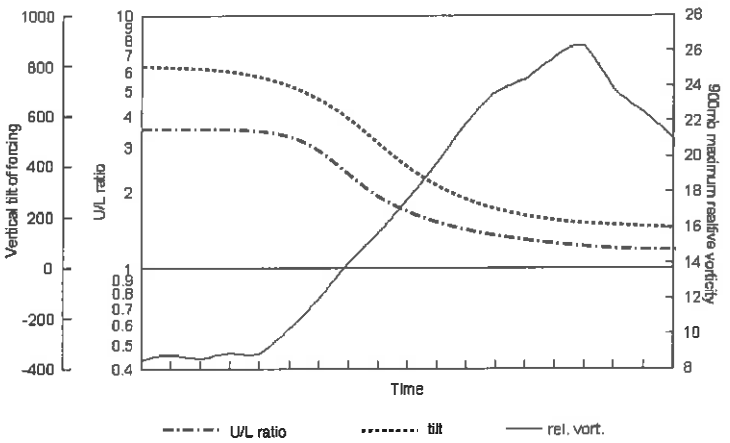

Figure 5: Graphs showing the time-history of the U/L ratio and vertical tilt of the forcing (in km), and also the 900hPa maximum relative vorticity (rel. vort. in $\times 10^{-5} s^{-1}$) for an idealised Type B cyclone.

R^2, is therefore used to define whether the cyclone has a Type B tilt regime (high correlation found) or a Type A tilt regime (low correlation).

In summary, it is expected that a Type A cyclone should have a small value for the average U/L ratio and show little correlation between the maximum 900hPa relative vorticity and the vertical tilt of the forcing during cyclogenesis. This is shown by the time-history plots in Fig. 4 for an idealised Type A cyclone. Type B cyclones, on the other hand, should have a large value for the average U/L ratio and show a relatively high correlation between the maximum 900hPa relative vorticity and tilt. This is shown by the time-history plots in Fig. 5 for an idealised Type B cyclone.

3 Results of classifying 16 cyclogenesis events

To produce an unbiased classification scheme, only cyclogenesis events that occurred during FASTEX (January - February 1997) were included. Only those events which underwent sustained development were used. The strength of the development was assessed using the value of the maximum relative vorticity at 900hPa. For a cyclone to be classified as having undergone sustained development, the 900hPa relative vorticity must have increased by $3.0 \times 10^{-5} s^{-1}$ over a twelve hour period while within the North Atlantic domain.

Sixteen such cyclogenesis events were identified during January and February 1997 (of which eleven were observed during FASTEX intensive observations periods, IOPs). These were examined using the methods described in Sec. 2.2. Table 3 shows the average U/L ratios and the correlation coefficient, R^2, as described in Sec. 2.2. Also shown is the probability, **p**, that a hypothesis of no correlation between relative vorticity and the vertical tilt of the forcing is correct. Using a 95% confidence level, if **p** is less than 0.05 then the correlation is significant. (The correlation coefficient and **p** are not shown for Low 30 and Low 41 in Table 3. This is because both these cyclones underwent two different periods of cyclogenesis which were separated by at least 12 hours. The average U/L ratio, R^2 and **p** for each cyclogenesis period of Lows 30 and 41 are given in Table 4 and are discussed later.)

Table 3 shows that there is a wide variation in the value of the U/L ratio. Some cases are dominated by upper-level forced vertical motion (e.g. Lows 18 and 44) while some have comparable amounts of upper and lower-level forced vertical motion (e.g. Lows 27 and 37). It should be remembered that, the ω_{QG} diagnostic has a reduced sensitivity to sources of vertical motion forced from lower-levels because of the boundary condition at the surface (Clough *et al.*, 1996) . Therefore when the U/L ratio less than or approximately equal to 1.0, this implies that forcing for vertical motion from lower levels is very strong and could be said to be dominating. Cyclogenesis events with an average U/L ratio less than 1.2 are assumed to be dominated by forcing for vertical motion from lower levels. The choice of this specific value, although somewhat arbitrary, is supported by the following analysis of the correlation coefficient. There appears to be a relationship in Table 3 between the value of the U/L ratio and R^2 (the correlation between the vertical tilt of the forcing and the maximum 900hPa relative vorticity). Cyclones with U/L ratios between 1.2 and 3.0 all show some correlation between the tilt and relative vorticity trends (shown by a value of **p** less than 0.05) while undergoing cyclogenesis: we shall argue that these correspond to Type B cyclones. Those

Type	Date	Low (IOP)	Ave. U/L	R^2	p
A	1-3 Feb. 97	Low 27 (9)	1.0	0.02	0.78
A	11-13 Feb. 97	Low 37 (14)	1.0	0.10	0.11
A	2-5 Feb. 97	Low 29	1.0	0.26	0.06
A	6-8 Feb. 97	Low 31	1.1	0.06	0.40
B	17-19 Feb. 97	Low 41 (17)	1.4		
B	8-10 Jan. 97	Low 8a (1)	1.5	0.68	0.00
B	13-15 Feb. 97	Low 38 (15)	1.6	0.56	0.02
B	4-7 Feb. 97	Low 30 (11)	1.7		
B	19-21 Feb. 97	Low 42A	1.8	0.98	0.01
B	8-9 Feb. 97	Low 33	2.0	0.99	0.00
B	22-23 Feb. 97	Low 42B	2.2	0.57	0.01
B	8-9 Feb. 97	Low 34A (12)	2.3	0.92	0.00
B	15-18 Feb. 97	Low 39A (16)	2.6	0.78	0.00
C	16-18 Feb. 97	Low 39B	3.4	0.22	0.17
C	16-19 Jan. 97	Low 18 (4)	3.9	0.01	0.97
C	21-23 Feb. 97	Low 44 (18)	4.2	0.23	0.12

Table 3: Averaged U/L ratio and correlation coefficient (R^2) between the 900mb relative vorticity and the vertical tilt of the forcing for all the cyclones examined, listed in reverse order of magnitude of U/L ratio. See Section 2.2 for definitions. Also shown is the probability, **p**, that the correlation was not significant.

Type	Date	Low (IOP)	Ave. U/L	R^2	p
~B	4-5 Feb. 97	Low 30 (11)	1.9	0.32	0.23
A	6 Feb. 97	Low 30 (11)	1.1	0.74	0.19
A	17-18 Feb. 97	Low 41 (17)	0.96	0.33	0.31
B	19 Feb. 97	Low 41 (17)	1.4	0.85	0.00

Table 4: Same as table 3 but for Lows 30 and 41, each subdivided into two separate periods of cyclogenesis.

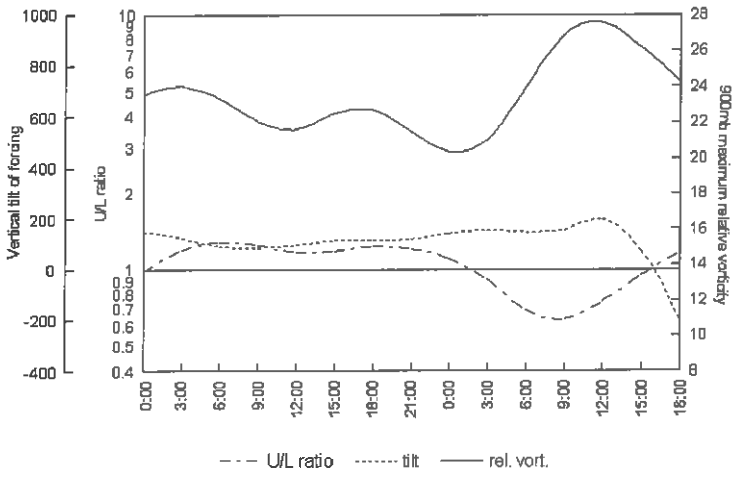

Figure 6: Graphs showing the time-history of the U/L ratio and vertical tilt of the forcing (in km), and also the 900hPa maximum relative vorticity (rel. vort. in $\times 10^{-5} s^{-1}$) for the Type A cyclone, Low 27 from 3UTC 1 Feb. 97 to 18UTC 3 Feb. 97.

cyclones with U/L ratios below 1.2 or above 3.0 show no significant correlation (**p** greater than 0.05). The low-level dominated cyclones, with average U/L ratios of less than 1.2 and no significant correlation correspond to PS71's Type A cyclones. The strongly upper-level dominated cyclones, with U/L ratios greater than 3.0 but with no significant correlation, correspond to neither Type A nor Type B. We refer to them as Type C and will discuss them later in this section.

Figure 6 shows graphs of the time series of the U/L ratio and separation measure for the ascent maxima (PF) associated with Low 27, the most low-level dominated cyclone observed. This graph shows that the U/L ratio associated with Low 27 remained close to 1.0 throughout the period in which the cyclone was within the North Atlantic domain. There was also an increase in the relative importance of the low-level forced ascent at 700hPa when the cyclone underwent cyclogenesis between 0UTC and 12UTC, 3 Feb. 97. The separation of the upper-level trough and cyclone, represented by the vertical tilt of the forcing, remained constant until the cyclone reached peak intensity at 12UTC, 3 Feb. 97. This all agrees closely with the PS71 definition of a Type A cyclone.

According to PS71, all upper-level forced cyclones should show a correlation between the cyclone's relative vorticity and the separation of the trough and cyclone (represented by the vertical tilt of the forcing), and they should fall into the Type B category. However, it can be seen from Table 3 that only the cyclones with U/L ratios between 1.2 and 3.0 displayed this correlation. Those cyclones that were strongly dominated by upper-level forcing (U/L ratio

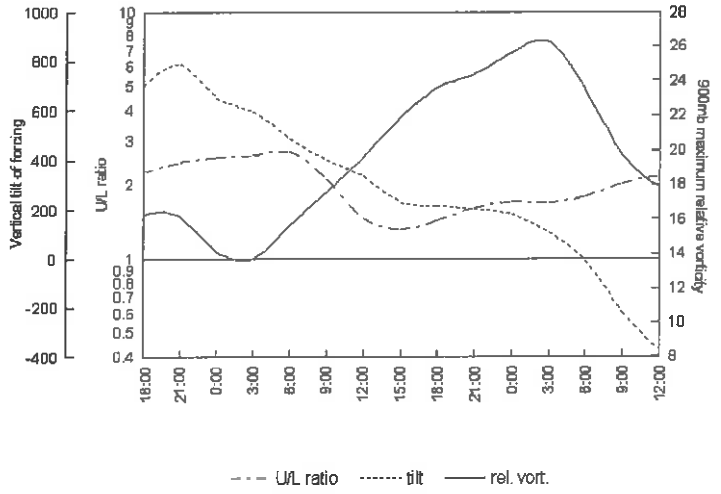

Figure 7: Graphs showing the time-history of the U/L ratio and vertical tilt of the forcing (in km), and also the 900hPa maximum relative vorticity (rel. vort. in $\times 10^{-5} s^{-1}$) for the Type B cyclone, Low 33 from 12UTC 7 Feb. 97 to 12UTC 9 Feb. 97.

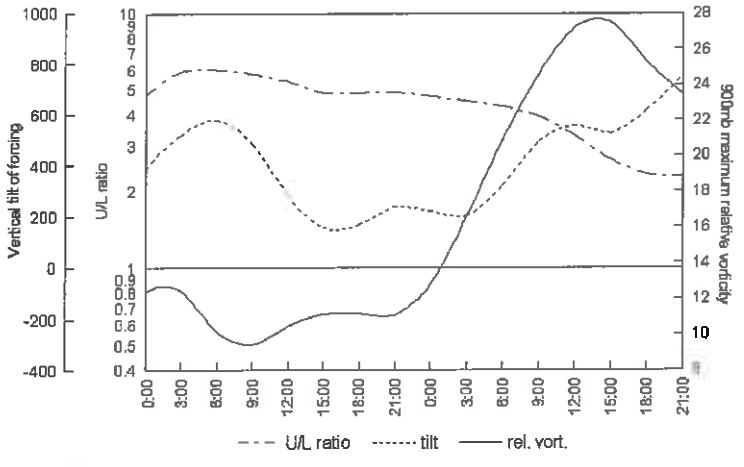

Figure 8: Graphs showing the time-history of the U/L ratio and vertical tilt of the forcing (in km), and also the 900hPa maximum relative vorticity (rel. vort. in $\times 10^{-5} s^{-1}$) for the Type C cyclone, Low 44 from 0UTC 22 Feb. 97 to 21UTC 23 Feb. 97.

greater than 3.0) showed no correlation between relative vorticity and tilt. This suggests that the upper-level forced cyclones may fall into two categories, identified in Table 3 as B and C. These two types are exemplified by Figs. 7 and 8 which show graphs of the U/L ratio and vertical tilt of the forcing associated with Lows 33 and 44, respectively. Low 33 is the cyclone event with the highest correlation between relative vorticity and separation, while Low 44 is the cyclone with the highest U/L ratio. Low 33 is a typical frontal wave development, triggered when an upper-level trough interacted with a trailing cold front. Figure 7 shows that Low 33 was characterised by initially high values of the U/L ratio. This ratio decreased sharply as cyclogenesis occurred due to an increase in thermal advection at low-levels. The separation between the trough and the cyclone (represented by the vertical tilt) was at a maximum when the frontal wave formed and decreased as the cyclogenesis proceeded. This cyclone was a prime example of a Type B cyclone as defined by PS71. (The earlier Figs. 2 and 3, relate to this case).

Figure 8 shows that Low 44 was initially strongly dominated by upper-level forced ascent. Although the U/L ratio did decrease as cyclogenesis occurred, it remained at a higher level than was seen in Low 33. There was also a distinct difference in the trend of the vertical tilt of the forcing. The tilt was close to a minimum as major cyclogenesis started and then increased as the low-level maximum relative vorticity increased. This indicated that when cyclogenesis was initiated the system displayed little westward tilt with height. However, the westward tilt increased as the cyclone intensified and the low-level forcing became relatively more important. Such an increase in tilt as the cyclogenesis occurred was found in all the cases with an U/L ratio greater than 3.0. This suggests a third category of extra-tropical cyclogenesis which was not included in PS71's scheme. To continue the notation of that scheme, this new, third category is referred to as Type C cyclogenesis. This category will be examined in more detail in Sec. 4.3 where it is shown to correspond to a polar-low type of cyclogenesis during its initial stages. Table 5 summarises the new extended version of PS71's classification scheme.

There were only two cyclones observed that did not fit easily into this scheme. These are the two cyclones, Low 30 and Low 41, shown earlier in Table 4 each of which underwent two periods of deepening. It seems from Table 4 that, in each case the deepening phases fell into very different regimes. It is suggested that both these cyclones were a hybrid of Type A and Type B cyclogenesis, with each cyclone undergoing periods of deepening corresponding

Cyclone Category	Ave. U/L ratio range	Tilt Correlation
Type A: low-level dominated	less than 1.2	weak
Type B: frontal wave cyclone	between 1.2 and 3.0	strong
Type C: upper-level dominated	greater than 3.0	weak

Table 5: An objective classification scheme of extra-tropical cyclones. "Ave. U/L ratio" is a measure of the relative importance of upper and lower level forcing averaged over the entire life time of the cyclone. "Tilt Correlation" refers to whether a correlation is found between the relative vorticity and the vertical tilt of forcing during cyclogenesis.

to the different categories. Low 30 does not fit into our classification scheme well in that the correlation (R^2) was not significant during its first period of cyclogenesis during which the averaged U/L ratio indicated it to be Type B.

4 Case studies to illustrate each cyclone category

This section presents a case study for each category and will relate the ω_{QG} diagnostics to the synoptic situation. For Type A and Type B cyclogenesis the case study will concentrate on the time of maximum development. For the new category, Type C, the whole life-cycle will be discussed in some detail. A review of the FASTEX IOPs, including overviews of all the cases discussed in this section can be found in Joly *et al.* (1999) and Clough *et al.* (1998).

Figure 9 shows satellite imagery and surface analysis for the three examples chosen to represent each of the main cyclone types (A, B and C) at the time of maximum deepening. Animations of similar plots (IR satellite imagery and objective fronts plotted at 900 and 600hPa) are available at the JCMM FASTEX workshop web site (http://www.met.rdg.ac.uk/FASTEX/wsindex.html) for all the cases discussed in this section. It is difficult to identify differences in the structure of these three different types of cyclone from conventional synoptic charts especially when viewed at only one time. However, in this section it will be shown that the key differences in the structure of the cyclones can be easily identified using the ω_{QG} diagnostics. There will also be discussion of the accuracy of the forecasts for each category based on the assessment of the accuracy of the UKMO

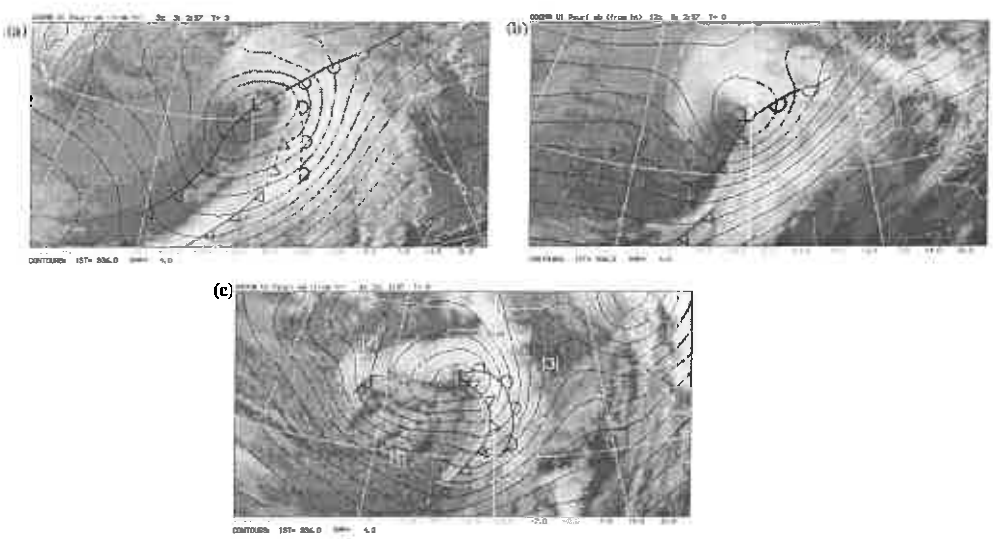

Figure 9: IR imagery from Meteosat overlaid with mean sea-level pressure contours (solid, every 4hPa) at the time of maximum deepening for (a) Low 27 (Type A) at 3UTC, 3 Feb. 97; (b) Low 33 (Type B) at 12UTC 8 Feb. 97; and (c) Low 44 (Type C) at 6UTC 23 Feb. 97 . The locations of the surface warm and cold fronts are based on those obtained from the objective plotting routine in Hewson (1998). Dashed fronts indicate the decaying fronts. The dashed white lines in (c) represent cloud features that began as three small comma clouds: [1] is represented by its axis and [2] and [3] by envelopes.

Unified Model in Clough *et al.* (1998) (also available at the above web site). The forecasts were validated at a time when each cyclone was in the so called MSA observing area (which consisted of the eastern part of the North Atlantic (Joly *et al.* (1997),(1999)) and were assessed on the basis of the error in the location and intensity of the surface low-pressure centre.

4.1 Low 27: an example of Type A cyclogenesis

An overview of the evolution of Low 27 using the ω_{QG} diagnostics was given in Fig. 6. This cyclone formed over North America before crossing the North Atlantic. From 18UTC 1 Feb. 97, there were indications that an occlusion was forming as the distance between the surface warm and cold fronts decreased. At this time Low 27 was a mature decaying cyclone. However, at 12UTC 2 Feb. 97 a secondary surface front developed and by 0UTC 3 Feb. 97 the surface warm front had intensified causing Low 27 to resemble an open frontal wave cyclone. This new warm front can be seen three hours later in Fig. 9(a) as the warm front upstream of the low centre. The original decaying frontal structure is also shown in this figure. By this time Low 27 had started to undergo cyclogenesis. Figure 6 indicates an increase in the relative strength of the low-level forced ω_{QG} at 700hPa and Fig. 10 shows

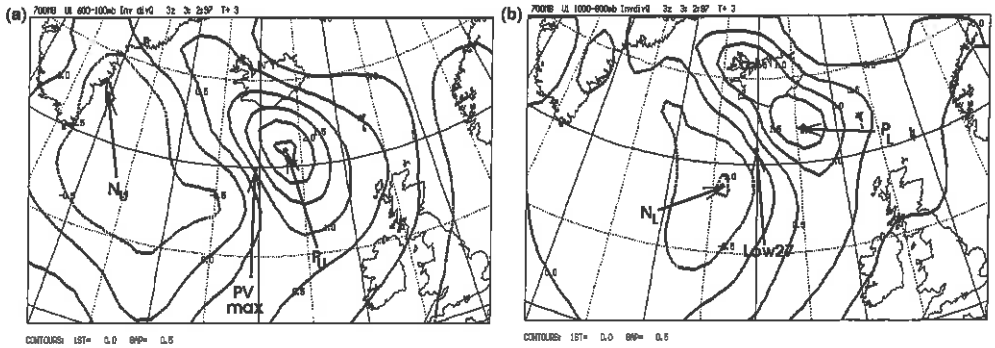

Figure 10: ω_{QG} at 700hPa forced from (a) upper-levels and (b) lower-levels associated with Low 27 at 3UTC, 3 Feb. 97 (solid contours, ascent; dashed contours descent, every $0.5cms^{-1}$). Low 27 is a Type A cyclone. P_U, N_U and P_L, N_L represent the location of the ascent and descent maxima at 700hPa forced from upper-levels and lower-levels, respectively. PV max is the location of the positive PV anomaly at 400hPa associated with the upper-level trough.

that the low-level forced ω_{QG} dipole at 700hPa had was the same order of magnitude and scale as the dipole forced from upper-levels. This implies that this period of deepening was mainly due to changes in the low-level thermal field. There was an upper-level trough and positive PV anomaly associated with the cyclone at this time. However, this PV anomaly had weakened during the proceeding 12 hours and did not begin to re-intensify until the cyclone had reached its peak intensity.

The other FASTEX cyclones in this category showed similar features when undergoing cyclogenesis. In particular, the re-development of the surface frontal structure was a clear indicator of the initiation of cyclogenesis. All the Type A cyclones examined also had a pre-existing upper-level trough but this was not a major factor in their development. Few cases of Type A cyclogenesis have been reported since the papers of Petterssen *et al.* (1962) and PS71. This may be due to the low-level forced cyclones that have been studied being unable to fulfill the excessively strict criterion that **no** upper-level trough should precede the cyclogenesis (Bluestein, 1993) . It is possible that owing to inadequate upper air data, Petterssen *et al.* (1962) were unable to identify relatively weak upper-level troughs behind the cyclones as observed in the low-level dominated cases here.

The forecast accuracy of two of the Type A cyclones examined here were discussed in Clough *et al.* (1998). Both Low 27 (IOP9) and Low 37 (IOP14) were well forecast by the operational Met. Office Unified Model, especially their location, up to T+120. The good accuracy in forecasting these Type A cyclones may be due to these cyclones forming over North America where there was a large amount of observational data. The accuracy of the

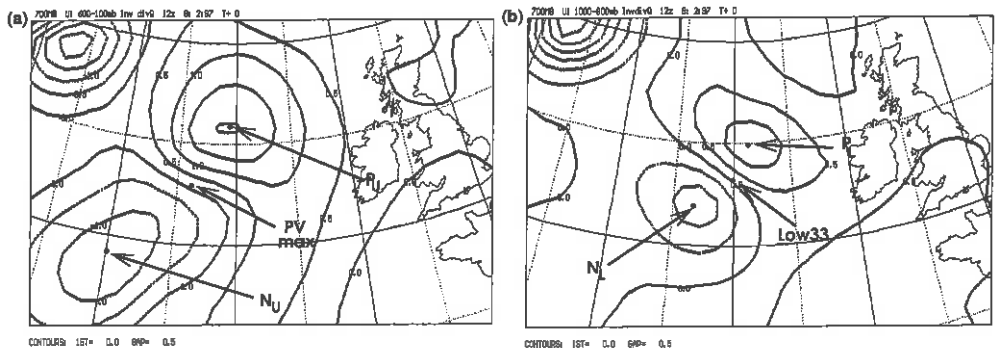

Figure 11: As for Fig. 10 but for the Type B cyclone, Low 33 at 12UTC, 8 Feb. 97.

forecasts could also have been influenced by the long-life time and slow evolution which is typical of Type A events.

4.2 Low 33: an example of Type B cyclogenesis

An overview of the evolution of Low 33 was given in Fig. 7. Low 33 was a small intense cyclone which crossed the Atlantic rapidly with an average speed of $23ms^{-1}$. The warm and cold fronts were of comparable strength and a cloud head and dry intrusion formed as it developed. The low was associated with its own upper-level positive PV anomaly. Figure 11 shows the ω_{QG} dipoles at 700hPa forced from upper and lower levels in association with Low 33 at the time of maximum rate of deepening. It is clear from the ω_{QG} fields that Low 33 was small in scale. The upper-level forced ω_{QG} dipole had a larger magnitude (see Table 2)and was of a greater scale than the lower-level forced dipole, indicating the dominance of the upper-level forcing. At this time the upper-level trough was close to the cyclone and the tilt of the system approached the vertical. This separation of the trough and cyclone had decreased throughout the development of Low 33 as expected for a Type B cyclone.

Type B cyclones were the most common type of cyclogenesis observed during FASTEX. They all involved the interaction of an upper-level trough with a low-level cyclone and its associated fronts in which the separation between the trough and cyclone decreased during cyclogenesis. It was also found that the Type B cyclones with higher U/L ratios tended to have stronger cold fronts than warm fronts and vice versa for Type B cyclones with lower U/L ratios than that for Low 33. The strength of the fronts was quantified by the magnitude of the gradient of θ_w across the front (as used by Hewson (1998) to identify

fronts objectively). Joly *et al.* (1999) found that all the Type B cyclones discussed here were initially second-generation waves on fronts. A large amount of research has been carried out on secondary frontal wave cyclones, most recently by Parker (1998), Rivals *et al.* (1998) and Chaboureau and Thorpe (1999).

Type B cyclones Lows 8(IOP1), 33(IOP11a), 34A(IOP12), 38(IOP15) and 39A(IOP16), were forecast with varying degrees of success during FASTEX. The location of these Type B cyclones tended to be well forecast for lead times out to three days. However, the accuracy of the predicted central pressure varied from good for Low 38 (error of -2hPa) to poor for Low 33 (error of +8hPa) in the 24 hour forecast. Low 38 had the largest scale of any of the Type B cyclones identified while Low 33 was one of the smallest. This indicates that the accuracy of the forecasts of Type B cyclones might be influenced by the scale of the system. All the Type B cyclones had significant errors in the central pressure for forecasts with lead times in excess of of three days and the formation of only a few were predicted beyond lead times of four days. This is likely to be due to their short life-cycle and the need for the location of both the upper-level trough and the low-level thermal gradient to be correctly predicted at the time of initiation. The forecasts were further hindered as Type B cyclones tended to be initiated over the ocean where there are fewer observations.

4.3 Low 44: an example of Type C cyclogenesis

Of the 16 cyclones studied, three were classified as exhibiting Type C cyclogenesis. Two of these, Lows 18 and 44, were designated FASTEX IOPs while the third low, Low 39B, was designated Lesser Observing Period, (LOP), 4. This section analyses Low 44 as a well-defined example of Type C cyclogenesis. Low 44 formed as an upper-level trough crossed the ice edge into the Labrador Sea at approximately 57°N, 55°W at 0UTC, 22 Feb. 97. Donnadile *et al.* (2000) have extensively examined the PV anomaly and tropopause fold associated with the upper-level trough. However, they did not examine the development of Low 44 that was forced by the upper-level trough.

Figure 9(c) shows the surface analysis and cloud imagery for Low 44 at 6UTC, 23 Feb. 97, as it underwent explosive development. Figure 12 shows the ω_{QG} dipoles at 700hPa forced from (a) upper and (b) lower levels in association with Low 44 at 6UTC, 22 Feb. 97, six hours after a low-level relative vorticity centre was first identified, but 24 hours before the time of maximum deepening shown in Fig. 9. When Low 44 formed, it had no significant

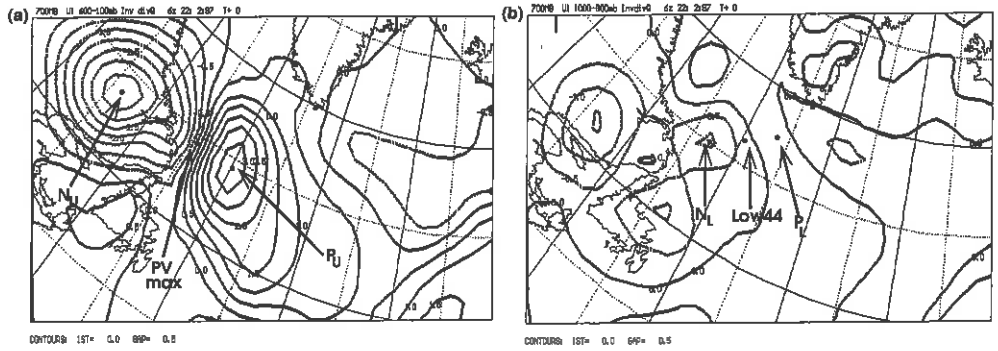

Figure 12: As for Figure 10 but for an example of Type C cyclogenesis just after initiation: Low 44 at 6UTC, 22 Feb. 97.

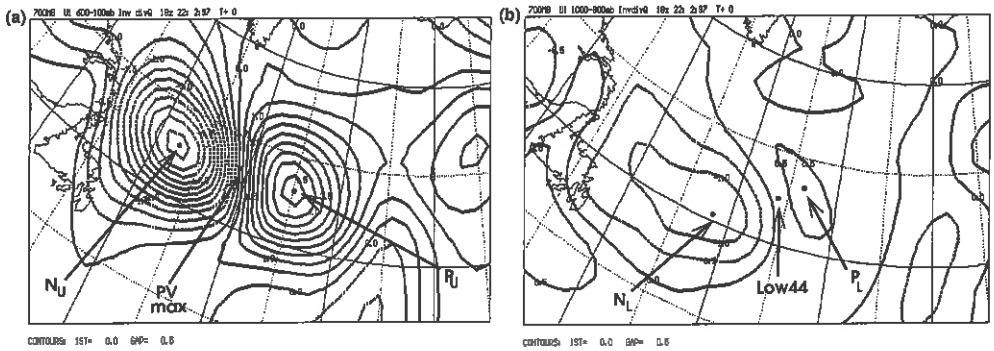

Figure 13: As for Fig. 10 but for Type C cyclogenesis prior to explosive deepening: Low 44 at 18UTC, 22 Feb. 97.

frontal structure although the 900hPa θ_w field (not shown) shows that there was a large region of cold air located upstream of the low centre. The upper-level trough associated with Low 44 was a short-wave feature embedded in a longer wave trough. The tropopause depression associated with this trough was the deepest observed during FASTEX, with the model-analysed PV2 surface descending to a height of 2.7km at 0UTC, 22 Feb. 97, when Low 44 crossed the ice edge. There was very little low-level forced ω_{QG} at this time but the upper-level forcing for ω_{QG} was strong enough for three organised convective cloud features resembling mesoscale comma clouds, denoted [1], [2] and [3] to form sequentially. The locations of [2] and [3] are outlined by the dashed white lines in Fig. 9(c), while the axis of the remains of the first convective cloud feature, [1], is shown by a short dashed line. Each of them formed in the same manner just ahead of the tropopause depression and rotated around it as it moved at a constant speed towards the east between the ascent maximum (P_U) and descent maximum (N_U) at 700hPa forced from upper-levels.

The evolution of the three comma clouds relative to the tropopause depression and other

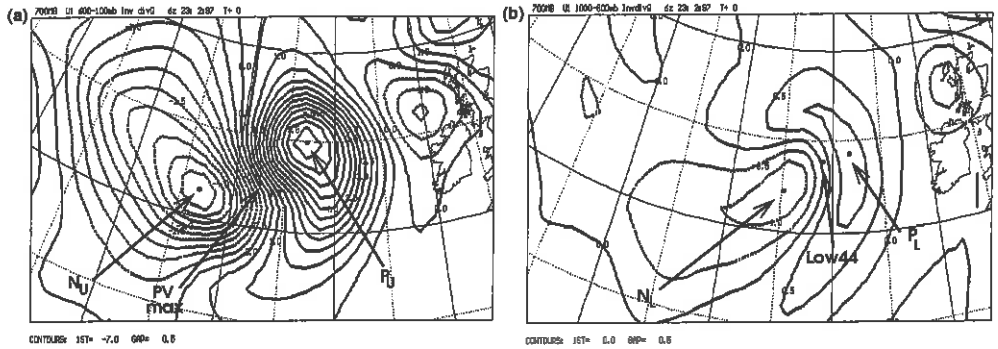

Figure 14: As for Fig. 10 but for Type C cyclogenesis during explosive deepening: Low 44 at 6UTC, 23 Feb. 97.

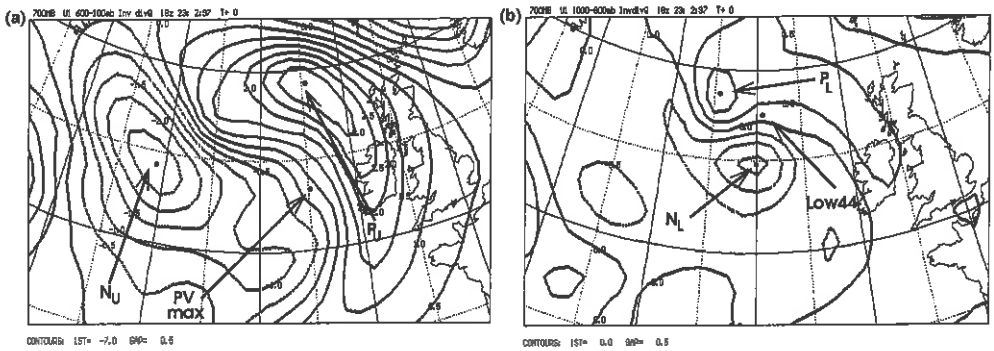

Figure 15: As for Fig. 10 but for Type C cyclogenesis at peak intensity: Low 44 at 18UTC, 23 Feb. 97.

features is depicted in the x-t (distance-time) diagram in Fig. 16 by defining an x-axis along the path of the tropopause depression and projecting features on to it at six hourly interval (all the features shown were within 500km of the x-axis). P_U, N_U and V represent the locations of the upper-level forced ascent and descent maxima at 700hPa and the PV maximum at 400hPa, respectively. The outlines of the three comma clouds, [1], [2] and [3], are also shown. According to Fig. 16 there was a constant spacing of approximately 500km between the comma clouds. The bold solid lines connect the successive positions of the centre of rotation of each of the comma clouds, the bold dashed lines connect the six-hourly locations of P_U and N_U and the dotted line connects the locations of the PV maximum. From this x-t diagram it can be seen that all the comma clouds formed close to P_U. The comma clouds [1] and [2] reached their maximum extent beneath V and decayed close to N_U. The average progression speed of [1] and [2] was significantly slower than that of the upper-level trough (the speed of [2] was $12.5ms^{-1}$ while the speed of the upper-level trough was $21.5ms^{-1}$). This behaviour indicated the absence of coupling between upper and lower levels. However, comma cloud [3] remained close to P_U as it developed and the

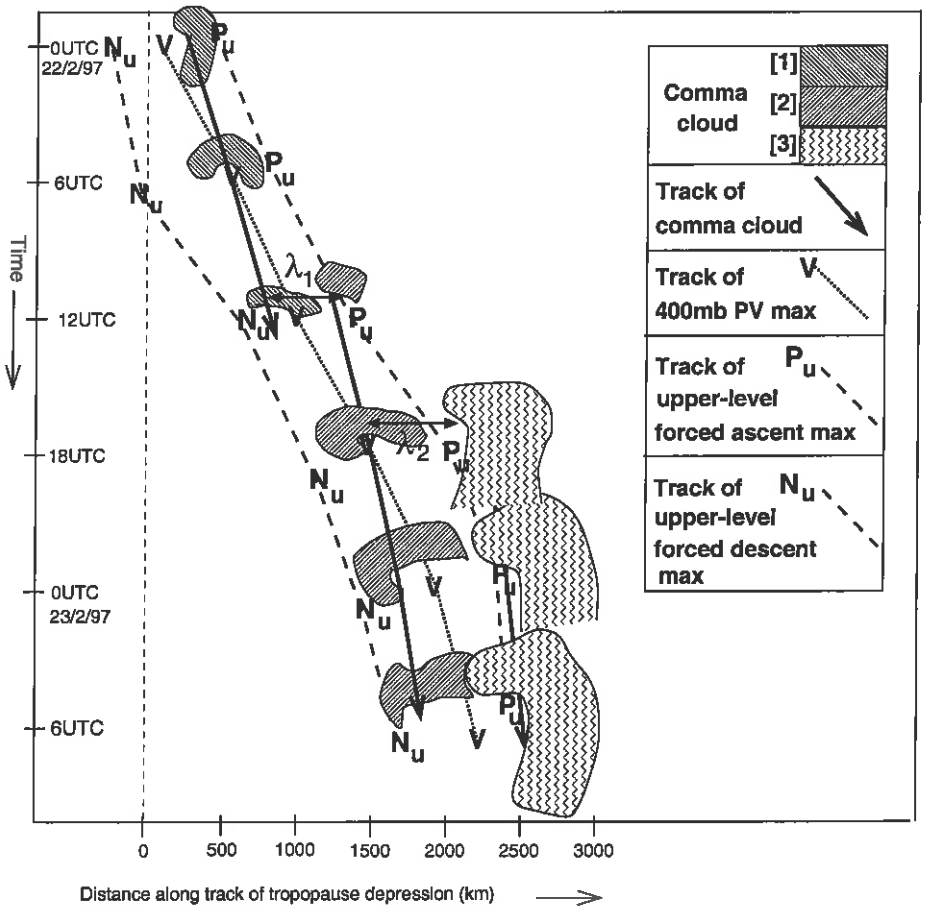

Figure 16: A distance-time diagram for Type C cyclone, Low 44, showing the development of the comma clouds (shaded) at 6-hour intervals relative to the location of the tropopause depression (V) and ascent and descent maxima at 700hPa, forced from upper-levels (P_U and N_U).

progression speed of the tropopause depression decreased, indicating that coupling between the upper and lower levels had at last been initiated. This occurred at the same time as Low 44 started to undergo explosive deepening and the low-level forced ω_{QG} increased.

Sequential development of comma clouds has been observed in earlier studies of polar lows by Shapiro *et al.* (1987). A separation between the comma clouds of 500km, similar to that observed for Low 44, has also been previously identified in observational polar low studies (Shapiro *et al.*, 1987) and theoretical studies (Montgomery and Farrell, 1992) . Prior to undergoing explosive development and before the upper and lower levels coupled, Low 44 had a very similar structure to a comma-cloud type polar low. Coupling occurred when low-level thermal advection was initiated. This had started by 6UTC, 23 Feb. 97 when Low 44 had started to deepen explosively. By this time fronts had formed and Low 44 had taken on a structure similar to a frontal-wave cyclone (see Fig. 9(c)). However, although the low-level forced ω_{QG} increased as the fronts formed, the upper-level forced ω_{QG} still dominated the development of Low 44 (Figure 15). Fig. 15 shows Low 44 at 18UTC, 23 Feb. 97 when it had reached its peak intensity. By this time Low 44 had transformed into a large frontal cyclone which dominated the North Atlantic basin.

Although examples of Type C cyclones of equivalent strength have been identified outside the FASTEX experiment, the other example of Type C cyclogenesis from FASTEX did not undergo such strong deepening. This reduced deepening rate was due the upper and lower levels not coupling. The coupling in Low 44 was triggered when the short-wave upper-level trough associated with Low 44 interacted with the long-wave trough axis which increased the meridional flow around the trough axis and led to thermal advection at low-level. Baehr *et al.* (1999) proposed a similar theory stating that the difference between Low 44 (IOP18) and Low 18 (IOP4) was that Low 44 met an area of pre-existing upper-level diffluence while Low 18 did not and so remained a non-developing comma cloud. The forecasts for both Low 18 and Low 44 were assessed by Clough *et al.* (1998). Forecasts of both lows were good up to a lead time of three days using the UKMO Unified Model. However, the longer-range forecasts were increasingly inaccurate, especially in predicting the location of the low centre. The strength of Low 44 was severely underestimated in the forecasts with lead times of five days or more.

5 Conclusions

A systematic and objective method is developed for applying the simple cyclone classification scheme developed by Petterssen and Smebye (1971). This method uses a height-attributable solution of the quasi-geostrophic (QG) ω equation to identify and quantify the relative importance of upper- and lower-tropospheric forcing and also the time trend in the horizontal spacing of the forcing at these two levels. By applying this classification method to an unbiased sample of cyclogenesis events from the FASTEX field experiment, the Type A and Type B scheme of Petterssen and Smebye (1971) is reproduced and extended to include a Type C. Type C cyclogenesis, consists of cyclones that form at high latitudes, when a large upper-level trough moves over the ocean. Initially these cyclones consist of organised convective features and have a similar structure to polar lows. However, if the upper-level trough interacts with another upper-level feature such as a long-wave trough axis or jet-streak, explosive development can occur. The cyclone then transforms into a large frontal cyclone with a prominent dry intrusion. Some cyclones underwent more than one period of development. In these cases it was found that each period of development could be classified into a different category. Two examples of this hybrid cyclogenesis were identified: one, Low 30, transformed from a Type B to a Type A cyclone while the second cyclone, Low 41, transformed from a Type A to a Type B cyclone.

A brief assessment of the forecasts of cyclones during FASTEX by the UKMO Unified Model, showed signs that forecast accuracy could be related to the type of cyclogenesis. Type A cyclones, in which the low-level atmospheric structure and forcing were critical, were the most accurately forecast due in part to their tendency to form over North America where there are many surface observations. However, for any Type A cyclones had form over oceans, accurate forecasts might still be expected, given the relatively dense surface network present over seas nowadays (compared to upper-levels). Synoptic scale forecasts of Type C cyclones were generally not as good as for Type A, especially for lead times in excess of three days. Given that upper-level structures are critical for Type C cyclones this is consistent with the density of observations being smaller, in general, for upper levels than lower levels. One consistent weakness in the forecasts for Type C cyclones was in capturing details of the mesoscale evolution (such as portrayed in Fig. 16) - this probably relates to the unstable tropospheric environment which presents problems when forecasting polar lows in general. Type B cyclones were the least well forecast, because of the need to represent

both the upper- and the lower-level structures accurately, as well as the timing (and hence location) at which any developmental interactions may occur.

These tentative results on forecast accuracy suggest there is scope for forecasting an error bound for a particular cyclone forecast, provided the cyclone type can be identified a priori. The method developed in this paper, using a height-attributable QG vertical motion diagnostics, is recommended as a suitable basis for identifying the cyclone type. This would have important practical implications for helping with predictability forecasts of severe (cyclone-related) weather events, such as very strong winds. The relationship between forecast accuracy and cyclogenesis regime needs to be investigated further using a larger database of cyclogenesis event. Automating the new classification method and using an automated tracking routine would make it possible to apply this approach operationally. There are some limitations to this classification method due to the domain dependence of the ω_{QG} diagnostics. Although the criteria distinguishing each type of cyclogenesis will remain the same whatever domain ω_{QG} is calculated over, the specified threshold values of the U/L ratios will change. For domains which include a large area of land, leading to higher domain-averaged static stability at lower levels, the threshold values of the U/L ratio will be higher than shown here.

Acknowledgements

We are grateful to Sid Clough at the Met Office for his help with the ω_{QG} diagnostics and to P.Panagi, E.Dicks and A.Macallan at JCMM for supplying the LAM data used in this paper. Abigail Deveson was supported by a CASE studentship from the Natural Environment Research Council and the Meteorological Office. The Joint Centre of Mesoscale Meteorology (JCMM) is supported by the Meteorological Office and the Department of Meteorology, University of Reading, and by the Natural Environment Research Council through its support of the Universities Weather Research Network.

References

Bader, M. F., Forbes, G. S., Grant, J. R., Lilley, R. B. E., and Waters, A. J., editors (1995). *Images in Weather Forecasting.* Cambridge University Press.

Baehr, C., Pouponneau, B., Ayrault, F., and Joly, A. (1999). Dynamical characteristics of the FASTEX cyclogenesis cases. *Quart. J. Roy. Meteor. Soc.*, **125**, 3469–3494.

Bluestein, H. B. (1993). *Synoptic-Dynamic Meteorology. Volume II, Observations and Theory of Weather Systems.* Oxford University Press.

Chaboureau, J.-P. and Thorpe, A. J. (1999). Frontogenesis and the development of secondary frontal wave cyclones in FASTEX. *Quart. J. Roy. Meteor. Soc.*, **125**, 925–940.

Clough, S. A. and Davitt, C. S. A. (1994). Development of an Atlantic frontal wave during IOP3 of Fronts92. In S. Gronas and M. A. Shapiro, editors, *The Life Cycles of Extratropical Cyclones; vol II*, pages 151–156, Geophysical Institute, University of Bergen. Proceedings of an International Symposium.

Clough, S. A., Davitt, C. S. A., and Thorpe, A. J. (1996). Attribution concepts applied to the omega equation. *Quart. J. Roy. Meteor. Soc.*, **122**, 1943–1962.

Clough, S. A., Lean, H. W., Roberts, N. W., Birkett, H., Chaboureau, J.-P., Dixon, R., Griffiths, M., Hewson, T. D., and Montani, A. (1998). A JCMM overview of FASTEX IOPs. *JCMM Internal Report*, **81**.

Donnadile, J., Cammas, J.-P., Mascart, P., Lambert, D., and Gall, R. (2000). FASTEX IOP18: A very deep tropopause fold. *Quart. J. Roy. Meteor. Soc.*, **126**, in press.

Evans, M. S., Keyser, D., Bosart, L. F., and Kackmann, G. M. (1994). A satellite derived classification scheme for rapid maritime cyclogenesis. *Mon. Wea. Rev.*, **122**, 1381–1416.

Hewson, T. D. (1998). Objective Fronts. *Meteorol. Appl*, **5**, 37–65.

Hodges, K. I. (1994). A general-method for tracking analysis and its application to meteorological data. *Mon. Wea. Rev.*, **122**, 2573–2586.

Hoskins, B. J. and Bretherton, F. P. (1972). Atmospheric frontogenesis models: mathematical formulation and solution. *J. Atmos. Sci.*, **29**, 11–37.

Hoskins, B. J., Draghici, I., and Davies, H. C. (1978). A new look at the ω equation. *Quart. J. Roy. Meteor. Soc.*, **104**, 31–38.

Joly, A., Jorgensen, D., Shapiro, M. A., Thorpe, A., Bessemoulin, P., Browning, K. A., Cammas, J. P., Chalon, J. P., Clough, S. A., Emanuel, K. A., Eymard, L., Gall, R., Hildebrand, P. H., Langland, R. H., Lemaitre, Y., Lynch, P., Moore, J. A., Persson, P.

O. G., Snyder, C., and Wakimoto, R. M. J. (1997). The Fronts and Atlantic Storm-Track Experiment (FASTEX): Scientific objectives and experimental design. *Bull. Amer. Met. Soc.*, **78**, 1917–1940.

Joly, A., Browning, K. A., Bessemoulin, P., Cammas, J. P., Caniaux, G., Chalon, J. P., Clough, S. A., Dirks, R., Emanuel, K. A., Eymard, L., Gall, R., Hewson, T., Hildebrand, P. H., Jorgensen, D., , Lalaurette, F., Langland, R. H., Lemaitre, Y., Mascart, P., Moore, J. A., Roux, P. O. G. P. F., Shapiro, M. A., Snyder, C., and Toth, Z. (1999). Overview of the field phase of the Fronts and Atlantic Storm-Track Experiment (FASTEX) project. *Quart. J. Roy. Meteor. Soc.*, **125**, 3131–3165.

McLennan, N. and Neil, L. (1988). Marine bombs program (phase II). Technical Report 88-002, Atmospheric Environment Service, Pacific Region.

Montgomery, M. T. and Farrell, B. F. (1992). Polar low dynamics. *J. Atmos. Sci.*, **49**, 2484–2504.

Panagi, P. M. and Dicks, E. M. (1997). Met. Office Unified Model data, diagnostics, graphics and other observational data, available from the JCMM under aegis of the Universities' Weather Research Network (UWERN). *JCMM Internal Report*, **69**.

Parker, D. (1998). Secondary frontal waves in the North Atlantic region: A dynamical perspective of current ideas. *Quart. J. Roy. Meteor. Soc.*, **124**, 829–856.

Petterssen, S. and Smebye, S. J. (1971). On the development of extratropical cyclones. *Quart. J. Roy. Meteor. Soc.*, **97**, 457–482.

Petterssen, S., Dunn, G. E., and Means, L. L. (1955). Report on an experiment in forecasting of cyclone developments. *J. Met*, **12**, 58–67.

Petterssen, S., Bradbury, D. L., and Pedersen, K. (1962). The Norwegian cyclone models in relation to heat and cold sources. *Geofys. Publ.*, **XXIV**, 243–280.

Rivals, H., Cammas, J.-P., and Renfrew, I. A. (1998). Secondary cyclogenesis: The initiation phase of a frontal wave observed over the eastern Atlantic. *Quart. J. Roy. Meteor. Soc.*, **124**, 243–267.

Roberts, N. M. (1998). How to use the display program DISP. *JCMM Internal Report*, **91**.

Shapiro, M. A., Fedor, L. S., and Hampel, T. (1987). Research aircraft measurement of a polar low over the Norwegian Sea. *Tellus series A*, **39**, 272–306.

Thorpe, A. J. and Bishop, C. H. (1995). Potential vorticity and the electrostatic analogy: Ertel-Rossby formulation. *Quart. J. Roy. Meteor. Soc.*, **121**, 1477–1495.

Weldon, R. B. (1979). Satellite training course notes. Part IV: Cloud patterns and the upper air wind field. Technical Report AWS/TR-79/003, 101pp, Air Weather Service.

Young, M. V. (1993). Cyclogenesis: Interpretation of satellite and radar images for the forecaster. *Forecasting Research Division Tech. Rep., UKMO*, **No. 73**.

CURRENT JCMM INTERNAL REPORTS

This series of JCMM Internal Reports, initiated in 1993, contains unpublished reports and also versions of articles submitted for publication. The complete set of Internal Reports is available from the National Meteorological Library on loan, if required.

1. **Research strategy and programme**
   K A Browning et al
   January 1993

2. **The GEWEX Cloud System Study (GCSS)**
   GEWEX Cloud System Science Team
   January 1993

3. **Evolution of a mesoscale upper tropospheric vorticity maximum and comma cloud from a cloud-free two dimensional potential vorticity anomaly**
   K A Browning
   January 1993

4. **The global energy and water cycle**
   K A Browning
   July 1993

5. **Structure of a midlatitude cyclone before occlusion**
   K A Browning and N Roberts
   July 1993

6. **Developments in systems and tools for weather forecasting**
   K A Browning and G Szejwach
   July 1993

7. **Diagnostic study of a narrow cold frontal rainband and severe winds associated with a stratospheric intrusion**
   K A Browning and R Reynolds
   August 1993

8. **Survey of perceived priority issues in the parametrizations of cloud-related processes in GCMs**
   K A Browning
   September 1993

9. **The effect of rain on longwave radiation**
   I Dharssi
   September 1993

10. **Cloud microphysical processes - a description of the parametrization used in the large eddy model**
    H Swann
    October 1993

11. **An appreciation of the meteorological research of Ernst Kleinschmidt**
    A J Thorpe
    May 1992

12. **Potential vorticity of flow along the Alps**
    A J Thorpe, H Volkert and Dietrich Heimann
    August 1992

13. **The representation of fronts**
    A J Thorpe
    January 1993

14. **A parametrization scheme for symmetric instability: test for an idealised flow**
C S Chan and A J Thorpe
February 1993

15. **The Fronts 92 Experiment: a Quicklook Atlas**
Edited by T D Hewson
November 1993

16. **Frontal wave stability during moist deformation frontogenesis**
Part 1: Linear wave dynamics
C H Bishop and A J Thorpe
May 1993

17. **Frontal wave stability during moist deformation frontogenesis**
Part 2. The suppression of non-linear wave development
C H Bishop and A J Thorpe
May 1993

18. **Gravity waves in sheared ducts**
S Monserrat and A J Thorpe
October 1993

19. **Potential vorticity and the electrostatics analogy: quasi-geostrophic theory**
C Bishop and A J Thorpe
November 1993

20. **Recent advances in the measurement of precipitation by radar**
A J Illingworth
April 1993

21. **Micro-physique et givrage: cloud microphysics and aircraft icing**
A J Illingworth
May 1993

22. **Differential phase measurements of precipitation**
M Blackman and A J Illingworth
May 1993

23. **Estimation of effective radius of cloud particles from the radar reflectivity**
N I Fox and A J Illingworth
May 1993

24. **A simple method of Dopplerising a pulsed magnetron radar**
A Hua, A J Illingworth and J Eastment
November 1993

25. **Radiation and polar lows**
George C Craig
February 1994

26. **Collected preprints submitted to the International Symposium on the Life Cycles of Extratropical Cyclones; Bergen, Norway, 27 June - 1 July 1994**
April 1994

27. **Convective frontogenesis**
Douglas J Parker and Alan J Thorpe
April 1994

28. **Improved measurement of the ice water content in cirrus using a total water evaporator**
Philip R A Brown and Peter N Francis
April 1994

29. **Mesoscale effects of a dry intrusion within a vigorous cyclone**
K A Browning and B W Golding
April 1994

30. **GEWEX Cloud System Study, Science Plan**
May 1994

31. **Parametrization of momentum transport by convectively generated gravity waves**
R Kershaw
May 1994

32. **Mesoscale Modelling Newsletter No 5**
May 1994

33. **Observations of the mesoscale sub-structure in the cold air of a developing frontal cyclone**
K A Browning, S A Clough, C S A Davitt, N M Roberts and T D Hewson
May 1994

34. **Longwave radiative forcing of a simulated tropical squall line**
Imtiaz Dharssi
July 1994

35. **On the nature of the convective circulation at a kata-cold front**
K A Browning
September 1994

36. **Collective preprints of papers submitted to the COST-75 International Seminar on Advanced Weather Radar Systems, Brussels, 20-23 September 1994**
November 1994

37. **Use of satellite imagery to diagnose events leading to frontal thunderstorms: Parts I and II of a case study**
K A Browning and N M Roberts
November 1994

38. **The role of spaceborne millimetre-wave radar in the global monitoring of ice cloud**
P R A Brown, A J Illingworth, A J Heymsfield, G M McFarquhar, K A Browning and M Gosset
December 1994

39. **Potential vorticity inversion**
Michal Ziemianski
October 1994

40. **Theory of mature tropical cyclones; a comparison between Kleinschmidt (1951) and Emanuel (1986)**
Suzanne L Gray
December 1994

41. **Dispersion and removal of pollutants during the passage of an atmospheric frontal system**
N R Gimson
December 1994

42. **The role of snow sublimation in frontogenesis**
D J Parker and A J Thorpe
December 1994

43. **Potential vorticity and the electrostatics Analogy: Ertel-Rossby formulation**
A J Thorpe and C H Bishop
December 1994

44. **Mesoscale aspect of extratropical cyclones: an observational perspective**
K A Browning
January 1995

45. **A polar low outbreak: evolution and mesoscale structures**
T D Hewson, G C Craig and C Claud
February 1995

46. **Generation of near-surface gusts of deep convection**
K Nakamura and R Kershaw
April 1995

47. **Attribution concepts applied to the Omega Equation**
S A Clough, C S A Davitt and A J Thorpe
June 1995

48. **Parametrization of mixed-phase cloud and precipitation**
Susan P Ballard and M Gerard Hutchinson
June 1995

49. **Short-range forecasting of stratocumulus: initialization prediction**
Susan P Ballard, Simon D Jackson and B Macpherson
June 1995

50. **Contributions of the JCMM/Dept of Meteorology Radar Group to the 27th AMS Radar Meteorology Conference, Vail October 1995**
June 1995

51. **Cold pools in shear**
Douglas J Parker
September 1995

52. **High-resolution analysis of frontal fracture**
K A Browning, S P Ballard and C S A Davitt
September 1995

53. **The albedo of broken cloud fields: calculations using a modified two stream radiation code**
Imtiaz Dharssi and Roy Kershaw
October 1995

54. **Parametrization of momentum transport by convection. I: theory and cloud modelling results**
R Kershaw and D Gregory
November 1995

55. **Variation of frontal structure along a cold front**
K A Browning and N M Roberts
November 1995

56. **Secondary frontal waves**
Douglas Parker
December 1995

57. **Objective fronts**
T D Hewson
March 1996

58. **Mesoscale analysis of the activation of a cold front during cyclogenesis**
K A Browning, N M Roberts and A J Illingworth
June 1996

59. **Investigation of different representations of rain in a 1-d evaporation model**
H Swann
May 1996

60. **Parametrization of diabatic processes in the inversion of the omega-equation**
M Athanassiadou and A J Thorpe
June 1996

61. **The role of the environmental flow in the development of secondary frontal cyclones**
I A Renfrew, A J Thorpe and A Joly
June 1996

62. **Consequences of the geostrophic momentum approximation on barotropic instability**
S Malardel, A J Thorpe and A Joly
June 1996

63. **Contributions to the AMS/RMS Conference on Mesoscale Processes**
Reading, 9-13 September 1996

64. **Vorticity and potential vorticity in stratified flows interacting with an isolated obstacle**
Jorge A Gutiérrez and A J Thorpe
September 1996

65. **Triple point development: two case studies**
Douglas Parker
September 1996

66. **Radar observations of wind-shear splitting within evolving atmospheric Kelvin-Helmholtz billows**
D Chapman and K A Browning
April 1997

67. **Cold frontal structure derived from radar wind profilers**
K A Browning, D Jerrett, J Nash, T Oakley and N M Roberts
May 1997

68. **The dry intrusion and its effect on the frontal, cloud and precipitation structure of extratropical cyclones**
K A Browning - Text of invited special lecture at the Spring Conference
of the Meteorological Society of Japan, University of Tsukuba, 22 May 1997

69. **Met. Office Unified Model data, diagnostics, graphics programs, and other observational data available from the JCMM through the aegis of the Universities Weather Research Network (UWERN).** (Plus supplement)
Peter Panagi and Ed Dicks
June 1997

70. **Contributions of the JCMM/Dept of Meteorology Radar Group to the 28th AMS Radar Meteorology Conference.** Austin, Texas
September 1997

71. **Sensitivity of short-range weather forecasts to local potential vorticity modifications**
Meral Demirtas and Alan Thorpe
July 1997

72. **Objective identification of frontal wave cyclones**
T D Hewson
August 1997

73. **Attribution and its application to mesoscale structure associated with tropopause folds**
A J Thorpe
September 1997

74. **The role of the environmental flow in the development of secondary frontal cyclones**
Ian A Renfrew, Alan J Thorpe and Craig H Bishop
September 1997

75. **Potential vorticity: a short history of its definitions and uses**
Alan J Thorpe and Hans Volkert
September 1997

76. **Superposing semi-geostrophic potential vorticity anomalies**
H R Birkett and A J Thorpe
September 1997

77. **Short period forecasting of catchment-scale precipitation.**
Part 1: the role of Numerical Weather Prediction
M A Pedder, M Haile and A J Thorpe
September 1997

78. **Verification of the tracking technique used in an experimental cloud motion wind inferring system**
Z Wang, K A Browning and G A Kelly
October 1997

79. **A preliminary study of Fourier series analysis for cloud tracking with GOES high temporal resolution images**
Z Wang
October 1997

80. **Analysis of an ex-tropical cyclone after reintensifying as a warm-core extratropical cyclone**
K A Browning, G Vaughan and P Panagi
November 1997

81. **A JCMM overview of FASTEX IOPs**
S A Clough, H W Lean, N M Roberts, H Birkett, J-P Chaboureau, R Dixon, M Griffiths, T D Hewson and A Montani
January 1998

82. **Programs for PV inversion and modification**
Meral Demirtas
December 1997

83. **Release of potential shearing instability in warm frontal zones**
D Chapman and K A Browning
February 1998

84. **The European Cloud-Resolving Modelling Programme (EUCREM)**
Summary Report from the coordinator
P W White
April 1998

85. **A frontal wave database**
T D Hewson
April 1998

86. **Layering observed in dropsoundings from IOP 1 of Fronts 92**
S A Clough
May 1998

87. **Use of wind-shear displays for Doppler radar data**
D Chapman and K A Browning
May 1998

88. **Radar estimates of rainfall rates at the ground in bright band and non-bright band events**
T J Smyth and A J Illingworth
June 1998

89. **Correction for attenuation of radar reflectivity using polarisation data**
T J Smyth and A J Illingworth
June 1998

90. **The effects of convection on chemical reactions and precipitation scavenging**
Neil R Gimson
July 1998

91. **How to use the display program DISP**
Nigel Roberts
August 1998

92. **Conceptual models of cyclogenesis**
Adrian T Semple
August 1998

93. **Observations of oblate hail using dual polarisation radar and implications for hail detection schemes**
T J Smyth, T M Blackman and A J Illingworth
September 1998

94. **The semigeostrophic diagnosis of vertical motion. Part I: Formulation and co-ordinate transformations**
Mike A Pedder and Alan J Thorpe
September 1998

95. **The semigeostrophic diagnosis of vertical motion. Part II: Results for an idealised baroclinic wave life cycle**
Alan J Thorpe and Mike A Pedder
September 1998

96. **Convective destabilisation by a tropopause fold diagnosed using potential vorticity inversion**
Morwenna Griffiths, Alan Thorpe and Keith Browning
October 1998

97. **Forecast skill of the ECMWF model using targeted observations during FASTEX**
A Montani, A J Thorpe, R Buizza and P Unden
October 1998

98. **Observations and model simulations of the FASTEX IOP 16 frontal wave - effects of sublimation**
Sid A Clough, Humphrey W Lean, Nigel M Roberts and Richard M Forbes
December 1998

99. **The application of conceptual models in NWP**
Adrian T Semple
January 1999

100. **Mesoscale analysis of arc rainbands in a dry slot**
K A Browning and N M Roberts
January 1999

101. **Interaction of mesoscale tropopause depressions with a warm-core cyclone: observational and model analyses, and sensitivity to analysis errors**
K A Browning, A J Thorpe, A Montani, D Parsons, M Griffiths, P Panagi and E M Dicks
February 1999

102. **The use of water vapour imagery and PV inversion to adjust initial conditions in NWP**
Sean J Swarbrick
February 1999
This report is no longer available; see Internal Report No.108

103. **Summary notes for a lecture course on Waves in the Atmosphere and Ocean**
A A White
March 1999

104. **Results of a questionnaire on the operational value of conceptual models (CMs) of fronts and cyclones**
N M Roberts & M V Young
July 1999

105. **Contributions to the Poster Session at the 1998 UWERN Annual Science Meeting**
assembled by A A White
August 1999

106. **The objective analysis of dropsonde data from FASTEX**
Richard Forbes, Sid Clough, Mark Dixon, Andy Macallan & Nigel Roberts
January 2000

107. *NWP Technical Report No.302*
Implications for Mesoscale Modelling from a Study of the FASTEX IOP 16 Mid-latitude Cyclone
Richard M Forbes, Humphrey W Lean, Nigel M Roberts and Peter A Clark
March 2000

108. *NWP Technical Report No.291*
The use of water vapour imagery and PV inversion to adjust initial conditions in NWP
Final Project Report
Sean J Swarbrick
September 1999

109. *NWP Technical Report No.294*
A guide to aspects of water vapour imagery interpretation: the significance of dry regions
Nigel M Roberts
January 2000

110. *NWP Technical Report No.300*
The relationship between water vapour imagery and thunderstorms
Nigel M Roberts
February 2000

111. *NWP Technical Report No.293*
Holomorphic structures in hydrodynamical models of nearly geostrophic flow
V N Roubtsov and I Roulstone
January 2000

112. *NWP Technical Report No.301*
Multi-sensor synthesis of the mesoscale structure of a cold-air comma cloud system
K A Browning, P Panagi and E M Dicks
March 2000

113. *NWP Technical Report No.307*
Observations of stratospheric air entering the circulation of a polar low
K A Browning and E M Dicks
May 2000

114. *NWP Technical Report No.309*
Wind profiler – Unified Model comparison statistics
Peter Panagi & Ed Dicks
March 2000

115. *NWP Technical Report No.310*
Towards a similarity theory of moist convective updrafts
Olaf Stiller and George C Craig
May 2000

116. *NWP Technical Report No.312*
The mystery of striated cloud heads in satellite imagery
R S Dixon, K A Browning and G J Shutts
April 2000

117. *NWP Technical Report No.313*
MDIAG: a Fortran 90 program to compute diagnostics on pressure levels from Unified Model data on model levels
Peter Panagi
June 2000

118. *NWP Scientific Paper No.56*
Rearrangements of functions with applications to meteorology and ideal fluid flow
R J Douglas
June 2000

119. *NWP Technical Report No.320*
Tests of New Dynamics Model on the FASTEX IOP16 case
Humphrey Lean
September 2000

120. *NWP Scientific Paper 57*
A classification of FASTEX cyclones using a height-attributable QG vertical motion diagnostic
A C L Deveson, K A Browing, T D Hewson
September 2000

Met Office Joint Centre for Mesoscale Meteorology Department of Meteorology
University of Reading PO Box 243 Reading RG6 6BB United Kingdom
Tel: +44 (0)118 931 8425 Fax: +44 (0)118 931 8791
www.metoffice.com